Three-color imaging differentiated ribosome association with masked and unmasked mRNAs (fig. S5A). β-actin mRNAs hybridized with a second-color probe after protease digestion revealed previously masked mRNAs (about half of the total). Masked mRNAs were associated with brighter ribosomal puncta, supporting the hypothesis that regions rich in ribosomes are part of the same masked complex (Fig. 2C and fig. S5, B to D).

Unbound and unmasked molecules should be washed away during permeablization of live neurons. Puromycin eliminated actively translating polysomes, followed by detergent extraction and fixation (fig. S6A). Large, bright ribosomal puncta were retained in dendrites, some containing single β-actin mRNAs; in contrast, glial cytoplasmic ribosomal signal was extracted (fig. S6, B to D and H). After cLTP in detergent-treated neurons, ribosome and β-actin mRNA FISH signal (Fig. 2D and fig. S6E) and the size of the optically reconstructed ribosomal puncta (fig. S6, F and G) decreased by about half, consistent with increased dispersal of ribosomes and mRNAs as a result of synaptic stimulation.

Increased ribosomal dispersal due to unmasking resulted in increased diffusion of ribosomes and mRNAs. To investigate dendritic rRNA dynamics, we employed spot photoactivation of a ribosomal protein (L10A) fusion. Immobile, bright structures surrounded single mRNAs (Fig. 2E). Photoactivated ribosome fusions exhibited diminished motility in dendrites relative to glial cells (Fig. 2G). After cLTP, quantification of ribosome dispersal from photoactivated sites revealed that the immobile ribosome fraction decreased (fig. S7B). Dendritic β-actin mRNAs were immobile, with a small portion undergoing active transport (*18*). Upon stimulation, immobile mRNAs exhibited corralled diffusion in their local environment (fig. S7, C and D), consistent with degranulation of a complex that prevents mRNA from diffusing until synaptic stimulation.

In addition to increased mRNA and ribosome dynamics, cLTP increased protein synthesis of a reporter for β-actin mRNA, consistent with unmasking that correlates with increased local β-actin translation (fig. S8). The protein FMRP has been shown to be a component of RNA granules and stalls ribosomes on mRNAs (*19*). *Fmr*1 knockout brains exhibit a reduction in the postpolysomal fractions (*20*), suggesting a role for *Fmr*1 in granule integrity. Accordingly, *Fmr*1 knockdown in culture decreased the abundance of masked β-actin mRNAs (fig. S9, A to C). We observed a similar effect in neurons isolated from knockout animals lacking the β-actin mRNA binding protein ZBP1 (fig. S9D).

In the model supported by this work, β-actin mRNA is present all along dendrites and is kept in a dormant state by packaging into inert structures ready to be locally activated. During synaptic stimulation, downstream effectors of signaling pathways locally prompt complex disassembly, putatively allowing active translation of mRNAs at activated synapses. This could be accomplished by regulation of self-aggregating protein motifs through posttranslational modifications (*21*) facilitating cycles of localized RNA granule formation and degranulation, thus making use of the same mRNAs repeatedly over time.

References and Notes

1. S. Ramón y Cajal, *Proc. R. Soc. London* **55**, 444–468 (1894).
2. A. Holtmaat, K. Svoboda, *Nat. Rev. Neurosci.* **10**, 647–658 (2009).
3. M. Matsuzaki, N. Honkura, G. C. Ellis-Davies, H. Kasai, *Nature* **429**, 761–766 (2004).
4. J. Tanaka *et al.*, *Science* **319**, 1683–1687 (2008).
5. B. Ramachandran, J. U. Frey, *J. Neurosci.* **29**, 12167–12173 (2009).
6. M. A. Sutton, E. M. Schuman, *Cell* **127**, 49–58 (2006).
7. T. Eom, L. N. Antar, R. H. Singer, G. J. Bassell, *J. Neurosci.* **23**, 10433–10444 (2003).
8. M. E. Klein, T. J. Younts, P. E. Castillo, B. A. Jordan, *Proc. Natl. Acad. Sci. U.S.A.* **110**, 3125–3130 (2013).
9. I. J. Cajigas *et al.*, *Neuron* **74**, 453–466 (2012).
10. A. M. Krichevsky, K. S. Kosik, *Neuron* **32**, 683–696 (2001).
11. G. Elvira *et al.*, *Mol. Cell. Proteomics* **5**, 635–651 (2006).
12. T. E. Graber *et al.*, *Proc. Natl. Acad. Sci. U.S.A.* **110**, 16205–16210 (2013).
13. Materials and methods are available as supplementary materials on *Science* Online.
14. D. Zenklusen, D. R. Larson, R. H. Singer, *Nat. Struct. Mol. Biol.* **15**, 1263–1271 (2008).
15. W. Lu *et al.*, *Neuron* **29**, 243–254 (2001).
16. Y. Kanai, N. Dohmae, N. Hirokawa, *Neuron* **43**, 513–525 (2004).
17. R. B. Knowles *et al.*, *J. Neurosci.* **16**, 7812–7820 (1996).
18. H. Y. Park *et al.*, *Science* **343**, 422–424 (2014).
19. J. C. Darnell *et al.*, *Cell* **146**, 247–261 (2011).
20. A. Aschrafi, B. A. Cunningham, G. M. Edelman, P. W. Vanderklish, *Proc. Natl. Acad. Sci. U.S.A.* **102**, 2180–2185 (2005).
21. T. W. Han *et al.*, *Cell* **149**, 768–779 (2012).

Acknowledgments: We thank G. J. Bassell for the gift of the Dendra-actin 3′UTR construct, J. Du Hoffmann for invaluable programming help, D. R. Larson for Localize software, and Y. J. Yoon for cloning L10A and helpful discussions. We also thank T. Trćek and other past and present members of the Singer lab for their suggestions and support. This work was supported by NIH grant NS083085-19 (formerly GM84364) and the Weisman Family Foundation. Author notes: A.R.B., B.W., and R.H.S. designed the experiments; A.R.B. performed the experiments; A.R.B. and B.W. performed optical engineering and data analysis; and A.R.B. and R.H.S. wrote the manuscript. Data in this paper are in partial fulfillment of the Ph.D. degree to A.R.B.

Supplementary Materials

www.sciencemag.org/content/343/6169/419/suppl/DC1
Materials and Methods
Figs. S1 to S9
References
FISH Probe Sequences
Movies S1 and S2

9 July 2013; accepted 4 December 2013
10.1126/science.1242939

Visualization of Dynamics of Single Endogenous mRNA Labeled in Live Mouse

Hye Yoon Park,[1,2] Hyungsik Lim,[3] Young J. Yoon,[1] Antonia Follenzi,[4,5] Chiso Nwokafor,[1,3,6] Melissa Lopez-Jones,[1] Xiuhua Meng,[1] Robert H. Singer[1,2,7,8]*

The transcription and transport of messenger RNA (mRNA) are critical steps in regulating the spatial and temporal components of gene expression, but it has not been possible to observe the dynamics of endogenous mRNA in primary mammalian tissues. We have developed a transgenic mouse in which all β-actin mRNA is fluorescently labeled. We found that β-actin mRNA in primary fibroblasts localizes predominantly by diffusion and trapping as single mRNAs. In cultured neurons and acute brain slices, we found that multiple β-actin mRNAs can assemble together, travel by active transport, and disassemble upon depolarization by potassium chloride. Imaging of brain slices revealed immediate early induction of β-actin transcription after depolarization. Studying endogenous mRNA in live mouse tissues provides insight into its dynamic regulation within the context of the cellular and tissue microenvironment.

Recent advances have provided insights into the behavior of RNA in real time (*1*). However, most live-cell imaging techniques require transfection or injection of exogenous reporters that are typically overexpressed or are missing regulatory elements and binding partners present in the endogenous molecules. Moreover, immortalized cells may not accurately exhibit RNA regulation representative of the native tissue environment.

To address these limitations, we generated a transgenic mouse in which all endogenous β-actin mRNA is fluorescently labeled by specific binding between the MS2 bacteriophage capsid protein (MCP) and the MS2 binding site (MBS) RNA stem-loops (*2*). Lentiviral transgenesis (*3*) was used to integrate the MCP-GFP (green fluorescent

[1]Department of Anatomy and Structural Biology, Albert Einstein College of Medicine, Bronx, NY 10461, USA. [2]Gruss-Lipper Biophotonics Center, Albert Einstein College of Medicine, Bronx, NY 10461, USA. [3]Department of Physics and Astronomy, Hunter College and Graduate Center of the City University of New York, New York, NY 10065, USA. [4]Department of Pathology, Albert Einstein College of Medicine, Bronx, NY 10461, USA. [5]Department of Health Sciences, University of Piemonte Orientale "A. Avogadro," Novara, Italy. [6]Department of Biological Sciences, Hunter College and Graduate Center of the City University of New York, New York, NY 10065, USA. [7]Dominick P. Purpura Department of Neuroscience, Albert Einstein College of Medicine, Bronx, NY 10461, USA. [8]Howard Hughes Medical Institute, Janelia Farm Research Campus, Ashburn, VA 20147, USA.

*Corresponding author. E-mail: robert.singer@einstein.yu.edu

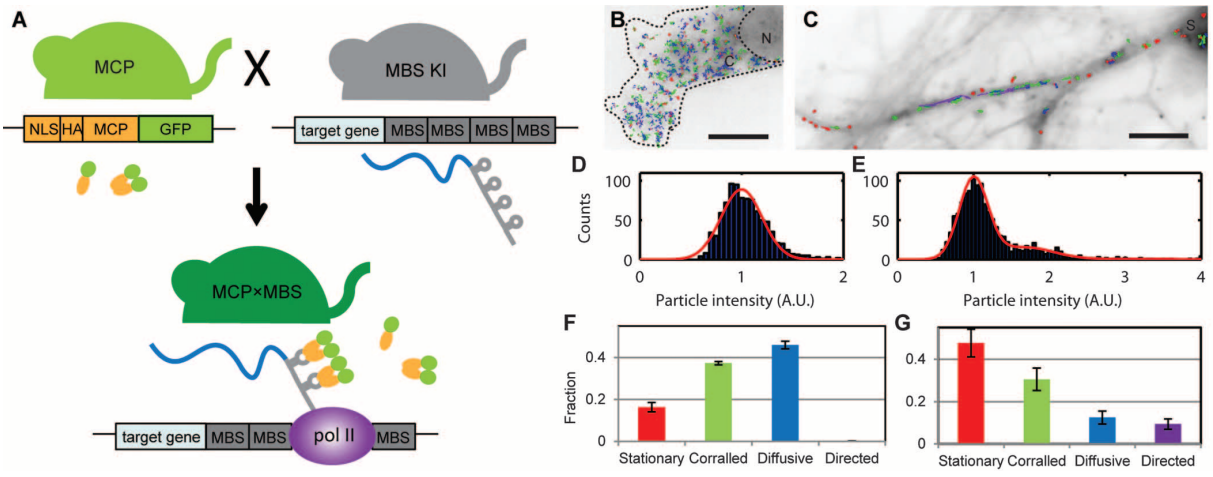

Fig. 1. Labeled endogenous mRNA in MCP×MBS mouse. (**A**) Schematic for in vivo RNA labeling. NLS, nuclear localization sequence; HA, hemagglutinin; pol II, RNA polymerase II. (**B** and **C**) Single-particle tracking of GFP-labeled β-actin mRNP in primary MEF (B) and hippocampal neuron (C) from mouse. Track classifications: red, stationary; green, corralled; blue, diffusive; purple, directed motion (see supplementary text). N, nucleus; C, cytoplasm; S, soma. Scale bars, 10 μm. (**D** and **E**) Intensity histograms of β-actin mRNPs tracked in primary MEFs (D) and neurons (E). Red curves show one- and three-component Gaussian fits for (D) and (E), respectively. (**F** and **G**) Fraction of stationary, corralled, diffusive, and directed β-actin mRNPs in primary MEFs (F) and neurons (G). Error bars denote SEM (n = 6 cells).

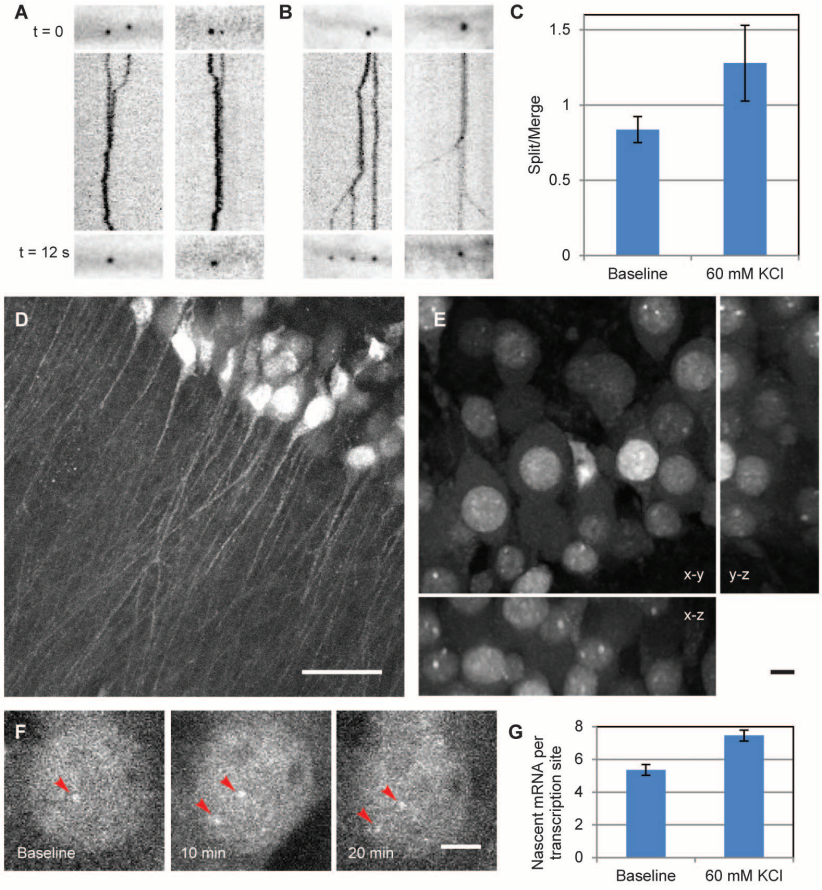

Fig. 2. Activity-dependent dynamics of β-actin mRNP in neurons from MCP×MBS mouse. (**A** and **B**) Examples of β-actin mRNP merge (A) and split (B) events. From top to bottom: initial images of the particles, kymographs during a 12-s period, and final images. (**C**) Ratio of split to merge events increased after KCl depolarization (n = 11 neurons from three cultures, 14 to 16 days in vitro; $P < 0.05$ by t test). (**D**) CA1 region in acute hippocampal slice. Scale bar, 50 μm. (**E**) Soma layer of CA1 neurons. Panels show maximum projections of x-y, y-z, and x-z planes. Scale bar, 10 μm. (**F**) Transcription of β-actin gene with KCl depolarization. Arrowheads denote β-actin transcription sites. Scale bar, 5 μm. (**G**) Nascent mRNA per transcription site increased after depolarization (n = 86 sites, brain slices from 3 mice; $P < 0.001$ by pairwise t test). Error bars denote SEM.

protein) transgene with high efficiency (fig. S1). The resulting MCP mice were crossed with Actb-MBS mice, in which 24 repeats of MBS are knocked into the 3′ untranslated region (UTR) of the β-actin gene (*4*), to label endogenous β-actin mRNA with GFP, resulting in MCP×MBS mice (Fig. 1A). β-Actin mRNA, which is essential for early embryonic development (*5*), was labeled with the 1200–nucleotide MBS cassette and up to 48 molecules of MCP-GFP (fig. S2A), yet no abnormalities were found by histologic analysis (n = 3 mice); mice were fertile (fig. S2B), and β-actin mRNA and protein expression levels were similar to those of wild-type mice (fig. S2, C and D). Hence, MS2-GFP labeling of endogenous β-actin mRNA did not disrupt its function and the expression level in vivo, confirming the physiological relevance of the studies.

Localization of β-actin mRNA was observed in primary fibroblast leading edges (*6*), neuronal growth cones (*7*), and mature neuron dendrites and spines (*8*) by fluorescence in situ hybridization (FISH). However, it is unclear how β-actin mRNA localizes in real time. Because loss of mRNA localization occurs in culture, we imaged mouse embryonic fibroblasts (MEFs) from MCP×MBS mice within 48 hours after isolation (Fig. 1B, fig. S3, and movie S1). Individual mRNA-protein complex (mRNP) particles were identifiable in MCP×MBS cells, unlike the background in MCP cells (fig. S2, E and F). Both single-molecule FISH and GFP labeling in live cells showed that these particles contained only single copies of β-actin mRNA (Fig. 1D, fig. S4, and supplementary text). The ensemble diffusion coefficient of the labeled endogenous β-actin mRNA was 0.09 ± 0.02 $\mu m^2/s$, similar to a reporter mRNA in a cell line (*9*). However, the movement patterns of endogenous mRNA appeared different from those of exogenous mRNA. There was less directed

motion (~1%) of endogenous mRNA (Fig. 1F and fig. S5) than previously reported (22%) (*9*), possibly due to the differences between the endogenous mRNA and the exogenous reporter, or the cell types. Serum-induced localization of β-actin mRNA in fibroblasts appears predominantly mediated by rapid release of stationary mRNA and redistribution into discrete cytoplasmic compartments (fig. S6, movies S2 to S5, and supplementary text), although we cannot rule out short movements driven by nonprocessive motors.

Neuronal RNA transport granules may contain multiple mRNAs (*10*, *11*). To investigate the stoichiometry of β-actin mRNA in hippocampal neurons from MCP×MBS mice, we performed single-molecule FISH (fig. S7). The intensity histograms of diffraction-limited fluorescent spots indicated mRNPs containing multiple copies of β-actin mRNA in the soma and proximal dendrites (fig. S7B), which decreased with distance from the soma (fig. S7D). In live neurons (Fig. 1C and movie S6), ~25% of mRNPs in proximal dendrites contained more than one β-actin mRNA (Fig. 1E). Diffusion of mRNPs in neurons was slower [diffusion coefficient = 3.8 (±0.5) × 10^{-3} $\mu m^2/s$] than in fibroblasts, but ~10% of mRNPs were actively transported anterograde and retrograde (Fig. 1G and fig. S8A) with a mean speed of 1.3 μm/s (fig. S8B). The ratio of anterograde to retrograde transport was 1.1 to 1.5 throughout neuronal development in culture (fig. S8C), which may mediate constitutive delivery into dendrites.

To investigate the activity-dependent dynamics of β-actin mRNA, we imaged live neurons before and after depolarization (60 mM KCl for 3 to 6 min). Pairwise comparisons in the same dendritic regions revealed that there were significant increases in the density of the mRNP particles after KCl depolarization in both cultured neurons (fig. S9) (*8*) and acute brain slices (fig. S10). The diffusion coefficient decreased by a factor of 3 (fig. S9D), and particles with directed motion decreased in both directions (fig. S9E). Therefore, the increase of diffraction-limited spots in the dendrite was not due to transport of mRNA from the soma. We hypothesized that the number of detected spots increased because of the release of mRNAs from mRNP complexes upon stimulation. We quantified the number of β-actin mRNAs contained in each neuronal mRNP by particle intensity. After KCl depolarization, the number of spots containing single β-actin mRNA increased while the number of particles bearing multiple mRNAs decreased (fig. S9B and S10B). We observed merge and split events of particles (Fig. 2, A and B, and movies S7 and S8). Both the split and merge frequencies were reduced after depolarization, but the ratio of split to merge was increased (Fig. 2C). These results suggest that mRNA molecules undergo continuous assembly and disassembly of large mRNP complexes (*12*) but favor the released state upon depolarization, possibly for local translation (*13*, *14*).

We investigated endogenous β-actin gene expression in native tissue by imaging acute brain slices (Fig. 2D). Transcriptional activity was monitored in the hippocampus CA1 region at 20 to 60 μm from the surface before and after KCl depolarization (Fig. 2E). Nascent β-actin mRNA per transcription site increased 10 to 15 min after depolarization (Fig. 2, F and G), likely because of rapid initiation (*15*). Rapid induction of β-actin transcription was observed in various cell lines (*4*, *16*, *17*) but β-actin was not recognized as an immediate early gene in the nervous system, probably because of high basal expression. Increased expression of β-actin may be implicated in transducing synaptic activity into structural plasticity.

The MCP×MBS mouse provides a distinctive tool for monitoring the dynamics of single endogenous mRNA in live mammalian cells and tissues. Our results with the β-actin gene suggest that the technique could be generally applicable to other genes to investigate the effect of the tissue microenvironment on single-cell gene expression.

References and Notes

1. S. Tyagi, *Nat. Methods* **6**, 331–338 (2009).
2. E. Bertrand *et al.*, *Mol. Cell* **2**, 437–445 (1998).
3. C. Lois, E. J. Hong, S. Pease, E. J. Brown, D. Baltimore, *Science* **295**, 868–872 (2002).
4. T. Lionnet *et al.*, *Nat. Methods* **8**, 165–170 (2011).
5. T. M. Bunnell, B. J. Burbach, Y. Shimizu, J. M. Ervasti, *Mol. Biol. Cell* **22**, 4047–4058 (2011).
6. J. B. Lawrence, R. H. Singer, *Cell* **45**, 407–415 (1986).
7. G. J. Bassell *et al.*, *J. Neurosci.* **18**, 251–265 (1998).
8. D. M. Tiruchinapalli *et al.*, *J. Neurosci.* **23**, 3251–3261 (2003).
9. D. Fusco *et al.*, *Curr. Biol.* **13**, 161–167 (2003).
10. K. Ainger *et al.*, *J. Cell Biol.* **123**, 431–441 (1993).
11. R. B. Knowles *et al.*, *J. Neurosci.* **16**, 7812–7820 (1996).
12. C. P. Brangwynne *et al.*, *Science* **324**, 1729–1732 (2009).
13. A. M. Krichevsky, K. S. Kosik, *Neuron* **32**, 683–696 (2001).
14. A. R. Buxbaum, B. Wu, R. H. Singer, *Science* **343**, 419–422 (2014).
15. D. R. Larson, D. Zenklusen, B. Wu, J. A. Chao, R. H. Singer, *Science* **332**, 475–478 (2011).
16. A. M. Femino, F. S. Fay, K. Fogarty, R. H. Singer, *Science* **280**, 585–590 (1998).
17. M. E. Greenberg, E. B. Ziff, L. A. Greene, *Science* **234**, 80–83 (1986).

Acknowledgments: Supported by NIH grants EB13571 and NS083085-19 (formerly GM84364) (R.H.S.) and National Research Service Award F32-GM87122 and the Integrated Imaging Program (H.Y.P.).

Supplementary Materials

www.sciencemag.org/content/343/6169/422/suppl/DC1
Materials and Methods
Supplementary Text
Figs. S1 to S10
Movies S1 to S8
References (*18*–*36*)

16 April 2013; accepted 15 October 2013
10.1126/science.1239200

The HydG Enzyme Generates an $Fe(CO)_2(CN)$ Synthon in Assembly of the FeFe Hydrogenase H-Cluster

Jon M. Kuchenreuther,[1]* William K. Myers,[1]* Daniel L. M. Suess,[1] Troy A. Stich,[1] Vladimir Pelmenschikov,[2] Stacey A. Shiigi,[3] Stephen P. Cramer,[1,4] James R. Swartz,[3,5] R. David Britt,[1]† Simon J. George[1]†

Three iron-sulfur proteins—HydE, HydF, and HydG—play a key role in the synthesis of the $[2Fe]_H$ component of the catalytic H-cluster of FeFe hydrogenase. The radical *S*-adenosyl-L-methionine enzyme HydG lyses free tyrosine to produce *p*-cresol and the CO and CN^- ligands of the $[2Fe]_H$ cluster. Here, we applied stopped-flow Fourier transform infrared and electron-nuclear double resonance spectroscopies to probe the formation of HydG-bound Fe-containing species bearing CO and CN^- ligands with spectroscopic signatures that evolve on the 1- to 1000-second time scale. Through study of the ^{13}C, ^{15}N, and ^{57}Fe isotopologs of these intermediates and products, we identify the final HydG-bound species as an organometallic $Fe(CO)_2(CN)$ synthon that is ultimately transferred to apohydrogenase to form the $[2Fe]_H$ component of the H-cluster.

FeFe hydrogenase enzymes rapidly evolve H_2 at a 6-Fe catalytic site termed the H-cluster (Fig. 1A) (*1*–*3*), which comprises a traditional 4Fe-4S subcluster ($[4Fe\text{-}4S]_H$), produced by canonical Fe-S cluster biosynthesis proteins, that is linked via a cysteine bridge to a dinuclear Fe subcluster ($[2Fe]_H$) that contains unusual ligands. Specifically, the $[2Fe]_H$ subcluster possesses two terminal CN^- ligands, two terminal CO ligands, and azadithiolate and CO bridges, all of which are thought to be synthesized and installed by a set of Fe-S proteins denoted HydE, HydF, and HydG. In one recent model for the $[2Fe]_H$ subcluster bioassembly pathway (*4*, *5*), the two radical *S*-adenosyl-L-methionine (SAM) enzymes of the set, HydE and HydG, generate the dithiolate moiety and free CO and CN^-, respectively, and these ligands are then transferred to a dinuclear Fe precursor bound to HydF,

[1]Department of Chemistry, University of California, Davis, Davis, CA 95616, USA. [2]Institut für Chemie, Technische Universität Berlin, Berlin 10623, Germany. [3]Department of Bioengineering, Stanford University, Stanford, CA 94305, USA. [4]Physical Biosciences Division, Lawrence Berkeley National Laboratory, Berkeley, CA 94720, USA. [5]Department of Chemical Engineering, Stanford University, Stanford, CA 94305, USA.

*These authors contributed equally to this work.
†Corresponding author. E-mail: rdbritt@ucdavis.edu (R.D.B.); sjgeorge@ucdavis.edu (S.J.G.)